Photocatalysis for Water Decomposition by RuO_2-Dispersed $ZnGa_2O_4$ with d^{10} Configuration

K. Ikarashi, J. Sato, H. Kobayashi,† N. Saito, H. Nishiyama, and Y. Inoue*

Department of Chemistry, Nagaoka University of Technology, Nagaoka 940-2188, Japan and Department of Chemistry and Bioscience, Kurashiki University of Science and the Arts, Kurashiki 712-8505, Japan

Received: February 26, 2002; In Final Form: June 2, 2002

The photocatalytic activity for water decomposition of RuO_2-dispersed $ZnGa_2O_4$ with an octahedrally coordinated Ga^{3+} ion was studied in order to examine the photocatalytic properties of p-block metal oxides with d^{10} configuration. $ZnGa_2O_4$ was impregnated with $Ru_3(CO)_{12}$ or $Ru(C_5H_7O_2)_3$ in THF and oxidized to convert them to RuO_2. For RuO_2-loaded $ZnGa_2O_4$, hydrogen and oxygen were stably produced from the initial stage of reaction under Hg−Xe lamp light irradiation. The activity dependence on the calcination temperature of $ZnGa_2O_4$, the amount of RuO_2 loaded, and the oxidation temperature of RuO_2 showed that the dispersion of small RuO_2 particles leads to high photocatalytic activity. The electronic structure of $ZnGa_2O_4$ was calculated by a plane-wave-based density function theory (DFT). The valence bands were mainly composed of the O 2p orbitals, whereas the conduction bands were formed by hybridzation of Ga 4s4p and Zn 4s4p orbitals. Large dispersion observed in the conduction band indicated the large mobility of photoexcited electrons, which was considered to be responsible for high photocatalytic performance. The feature of electronic structures relating to photocatalysis was discussed in comparison with those of transition metal oxides.

Introduction

For the overall splitting of water by a solid photocatalyst system, almost all of the photocatalysts developed in the past two decades have been composed of transition metal oxides involving octahedrally coordinated d^0 metal ions[1−17] such as Ti^{4+}, Zr^{4+}, Nb^{5+}, and Ta^{5+}. These metal oxides have mostly been used by being combined with NiO or RuO_2 as a promoter.

Recently, we have found that the p-block metal oxides of MIn_2O_4,[18,19] M_2SnO_4,[18] and $M_2Sb_2O_7$ (M = Ca, Sr)[20] make good photocatalysts for water decomposition when RuO_2 particles were dispersed on these metal oxides. To our knowledge, these are the first studies demonstrating that metal oxides other than the d^0 transition metal oxides are photocatalytically active for water splitting to hydrogen and oxygen. The interesting feature is that MIn_2O_4, M_2SnO_4, and $M_2Sb_2O_7$ (M = Ca, Sr) are composed of octahedrally coordinated d^{10} metal ions of In^{3+}, Sn^{4+}, and Sb^{5+}, respectively. The discovery predicts that the other kinds of the elements in p-block metal oxides would have potential to offer photocatalysts, either by itself or by being combined with the promoters, which are able to produce H_2 and O_2 from water under light irradiation. In aiming at further establishing the role of the p-block metal oxides with d^{10} configuration in photocatalysis for water decomposition, we have paid attention to zinc gallate, $ZnGa_2O_4$, involving a Ga^{3+} metal ion and found that RuO_2-dispersed $ZnGa_2O_4$ is photocatalytically active for the overall splitting of water. The electronic structure of $ZnGa_2O_4$ was calculated based on a plane wave density function theory (DFT), and its role in photocatalysis was discussed. The features in the conduction bands different from those of conventional transition metal oxide photocatalysts have been pointed out.

* Corresponding author.
† Kurashiki University of Science and the Arts.

Experimental Section

Zinc gallate was synthesized by a solid-state reaction at high temperatures. For $ZnGa_2O_4$, an equimolar mixture of Ga_2O_3 (Soekawa Chemical Co, high purity, 4-N grade) and ZnO (Nakalai tesque, extra pure grade) was heated in air in the temperature range 1273−1473 K for 16 h. The formation of the metal oxides was confirmed by the X-ray diffraction patterns.[21] The preparation of RuO_2-loaded $ZnGa_2O_4$ was performed by an impregnation method using ruthenium complex, $Ru_3(CO)_{12}$ (Aldrich, 99%), or ruthenium acetyl acetonate, $Ru(C_5H_7O_2)_3$ (Merck Schuchardt, >99%), as starting materials. The prepared $ZnGa_2O_4$ was impregnated with either of two ruthenium compounds in THF, dried at 353 K, and subjected to oxidation in air from 373 to 773 K so as to convert the ruthenium species to ruthenium oxide. To distinguish two kinds of RuO_2 loaded, the notation of RuO_2 was used for ruthenium oxide prepared from $Ru_3(CO)_{12}$, and the symbol of (acac) was added to RuO_2, such as RuO_2(acac), in case that $Ru(C_5H_7O_2)_3$ was used. The weight percent of RuO_2 loaded was described by a metal content unless otherwise specified.

The photocatalytic reaction was performed in a closed gas-circulating apparatus equipped with a quartz reaction cell. About 250 mg of photocatalyst was placed in ion-exchanged and distilled water in the quartz reaction cell. The atmosphere in the reaction system was filled with 1.33 kPa of Ar gas and circulated with a glass piston pump. Powder photocatalysts were dispersed in the water by stirring of Ar gas bubbling and irradiated with 200 W Hg−Xe lamp light. H_2 and O_2 produced in the gas phase were analyzed by an on-line gas chromatograph.

The plane-wave-based density function theory (DFT) calculation was carried out employing the CASTEP program.[22] The core electrons were replaced with the ultra-soft core potentials, and the valence electronic configurations are $4s^23d$,[10] $4s^23d^{10}$-$4p^1$, and $2s^22p^4$ for Zn, Ga, and O, respectively. The kinetic

10.1021/jp020539e CCC: $22.00
Published on Web 08/08/2002

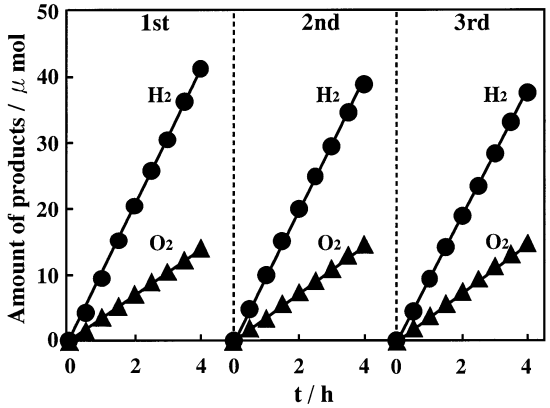

Figure 1. Water decomposition on 1 wt % RuO_2-dispersed $ZnGa_2O_4$. $ZnGa_2O_4$ was prepared by calcination at 1373 K. ●, H_2; ▲, O_2.

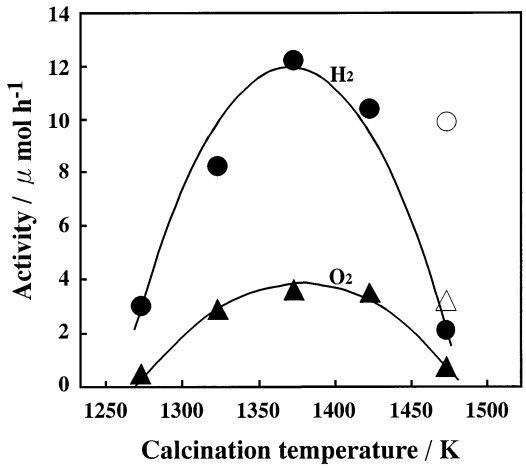

Figure 2. Changes in photocatalytic activity of RuO_2-dispersed $ZnGa_2O_4$ with calcination temperature of $ZnGa_2O_4$. ●, H_2; ▲, O_2 for 1 wt % RuO_2 loading; ○, H_2; △, O_2 for 0.6 wt % RuO_2 loading.

energy cutoff was taken to be 260 eV. The primitive unit cell was composed of $[ZnGa_2O_4]_2$, and the number of occupied orbitals was 62.

The X-ray photoelectron spectra of RuO_2-loaded $ZnGa_2O_4$ were recorded on a JEOL JPS-100SX using Mg Kα as an X-ray source. The binding energy was corrected by taking a C1s level as 284.5 eV. The UV reflectance spectra of $ZnGa_2O_4$ were recorded on a JASCO UVIDEC- 660 spectrometer. The scanning electron microscopic (SEM) images of $ZnGa_2O_4$ were obtained by a Shimazu-1600 spectroscope at a magnification of 5000.

Results

Figure 1 shows water decomposition on a 1 wt % RuO_2-dispersed $ZnGa_2O_4$ photocatalyst. Hydrogen and oxygen were produced in the gas phase from the initial stage of light irradiation, and their amounts increased in proportion to irradiation time. The second and third runs showed nearly the same production of both hydrogen and oxygen. The ratio of H_2/O_2 was considerably larger than the stoichiometric ratio of 2 in the initial run, but with photocatalytic run, the ratio decreased to approach the stoichiometric ratio.

Figure 2 shows changes in photocatalytic activity with the calcination temperature of $ZnGa_2O_4$. The photocatalytic activity was low when $ZnGa_2O_4$ was calcined at 1273 K, but increased with increasing calcination temperatures. The maximum activity was obtained by calcination at 1373 K, followed by a sharp decrease at temperatures higher than it. The photon efficiency

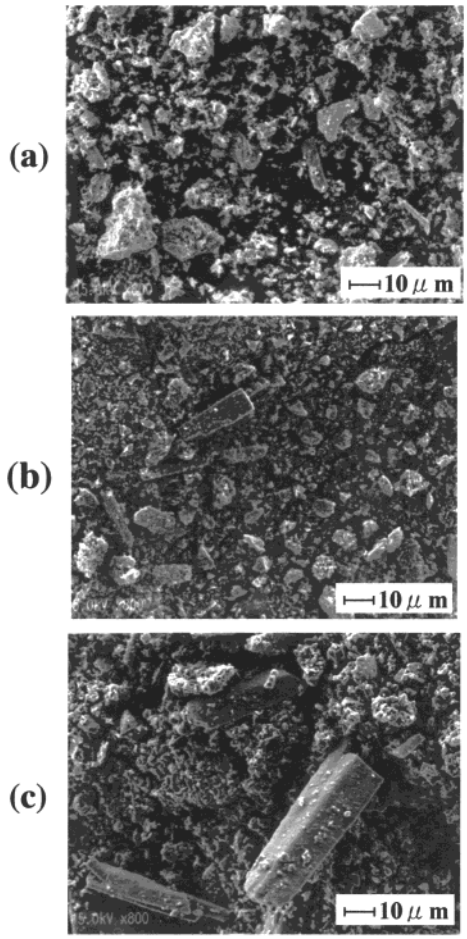

Figure 3. Scanning electron microscopic images of $ZnGa_2O_4$ treated by calcination at 1273 K (a), 1373 K (b), and 1473 K (c).

of RuO_2-dispersed $ZnGa_2O_4$ was very roughly estimated to be 4% from a comparison of the photocatalytic activity with previous results. Figure 3 shows the SEM images of $ZnGa_2O_4$ calcined at different temperatures. The particle sizes of 1273 K-calcined $ZnGa_2O_4$ provided irregular form, and the average particle size was 5 μm. The marked growth of particles occurred by calcination at 1473 K, leading to the formation of large particles, and the particle size increased to larger than 20 μm. In an EDS analysis for the composition of the particles, both small and large particles contained Zn and Ga elements consistent with the stoichiometric ratio of Ga/Zn within measurement errors, indicating that both particles are composed of $ZnGa_2O_4$, although their particle sizes were significantly different. The surface area measured by a BET method using nitrogen at 77 K was 2.3 $m^2\ g^{-1}$ for $ZnGa_2O_4$ calcined at 1273 K, 1.7 for 1373 K, and 0.7 for 1473 K. Figure 4 shows the X-ray diffraction patterns for $ZnGa_2O_4$ calcined at various temperatures. All the peaks observed were assigned to those reported previously.[21] The diffraction peaks became strong and sharp, indicating that crystallization proceeded in the temperature range from 1273 to 1473 K. To examine the influence of RuO_2-loading on the photocatalytic activity of $ZnGa_2O_4$ subjected to high calcination temperature, the amount of Ru loaded was reduced from 1 to 0.6 wt % for 1473 K-calcined $ZnGa_2O_4$. As shown in Figure 2, the activity of 0.6 wt % RuO_2-loaded $ZnGa_2O_4$ increased by a factor of 5, compared to 1 wt % RuO_2-loaded $ZnGa_2O_4$.

Figure 5 shows the dependence of photocatalytic activity on oxidation temperature to convert a Ru metal carbonyl complex to ruthenium oxide on a $ZnGa_2O_4$ surface. For $Ru_3(CO)_{12}$-

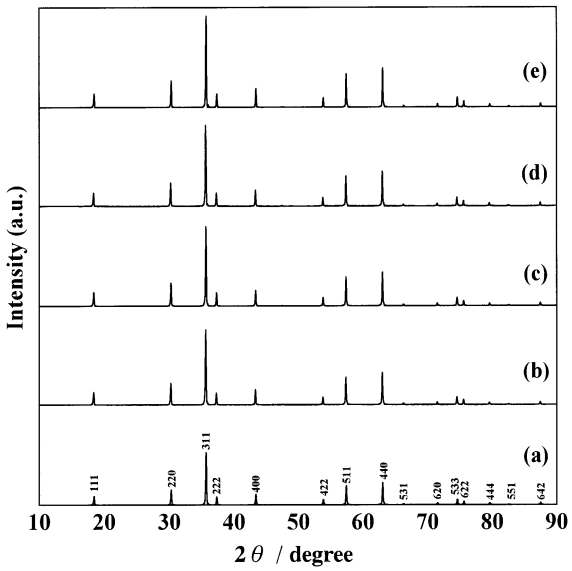

Figure 4. X-ray diffraction patterns of $ZnGa_2O_4$ calcined at 1273 K (a), 1323 K (b), 1373 K (c), 1423 K (d), and 1473 K (e).

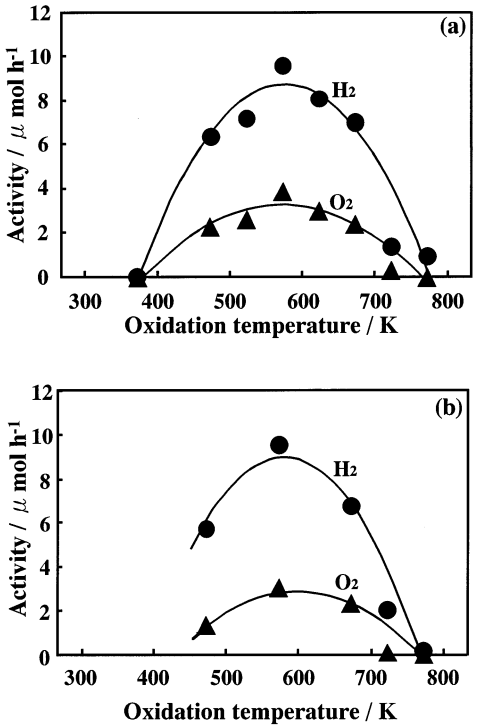

Figure 5. Photocatalytic activity dependence on oxidation temperature for RuO_2 formation from loaded $Ru_3(CO)_{12}$ (a) and for RuO_2(acac) formation from loaded $Ru(C_5H_7O_2)_3$ (b). ●, H_2; ▲, O_2

impregnation, the activity was negligible with an oxidation temperature of 373 K. It increased with increasing temperature, passed through a maximum by oxidation at 573 K, and decreased dramatically with the higher temperature. The XP spectra were taken for the Ru species with different oxidation temperatures. Table 1 shows the binding energy of Ru $3d_{5/2}$ level. The binding energy was 281.1 eV for Ru oxidized at 373 K and shifted toward lower binding energy by 0.4 eV with oxidation at 573 K. A slight positive shift occurred when oxidized at 723 K. For $Ru(C_5H_7O_2)_3$-impregnation, as also shown in Figure 5, the photocatalytic activity increased with increasing oxidation temperature, reached a maximum at 573 K, and decreased. Both the ruthenium species showed similar changes with oxidation temperature.

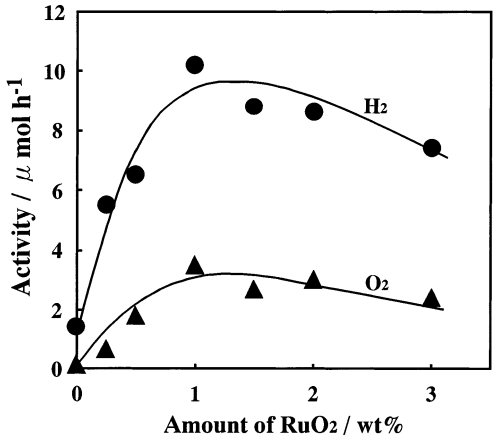

Figure 6. Photocatalytic activity as a function of RuO_2 amount. ●, H_2; ▲, O_2.

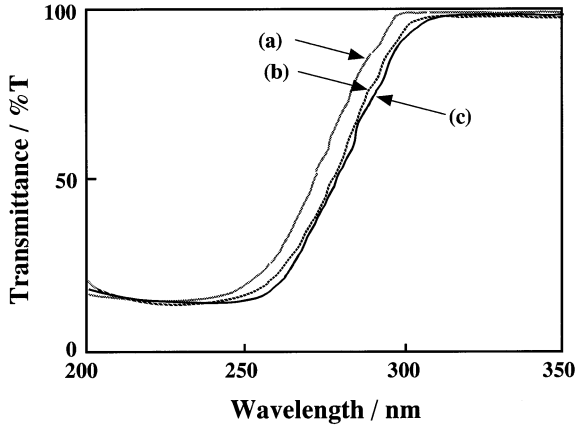

Figure 7. UV diffuse reflectance spectra of $ZnGa_2O_4$. $ZnGa_2O_4$ was subjected to calcination temperature of 1273 K (a), 1373K (b), and 1473 K (c).

TABLE 1: Binding Energy of Ru $3d_{5/2}$

samples	oxidation temperature/K	binding energy of Ru $3d_{5/2}$ level/eV	ref
Ru-impregnated	373	281.1	
$ZnGa_2O_4$	573	280.7	
	723	280.9	
Ru powder		280.1	2
	823	280.6	2
RuO_2 powder		280.7	2

Figure 6 shows the photocatalytic activity as a function of the amount of RuO_2 dispersed on $ZnGa_2O_4$. Without RuO_2-loading, only hydrogen was produced and its activity was quite small, while oxygen production occurred in the presence of a small amount of RuO_2. The activity for hydrogen and oxygen production increased with an increasing amount of RuO_2, passed through a maximum at around 1 wt %, and decreased considerably with further loading.

Figure 7 shows the UV diffuse reflectance spectra of $ZnGa_2O_4$ subjected to different calcination temperatures. Light absorption started at around 300 nm, increased steeply at around 280 nm and reached a maximum level at 250 nm. With increasing calcination temperature, the absorption band slightly shifted toward higher wavelength.

Figure 8 shows the energy-band diagram and the density of states (DOS) for $ZnGa_2O_4$ evaluated by the DFT calculation. In DOS, the first and second bands with the lowest energies were due to the O 2s and Ga 3d orbitals, respectively. The third band (i.e., the valence band) was rather broad whose lower part

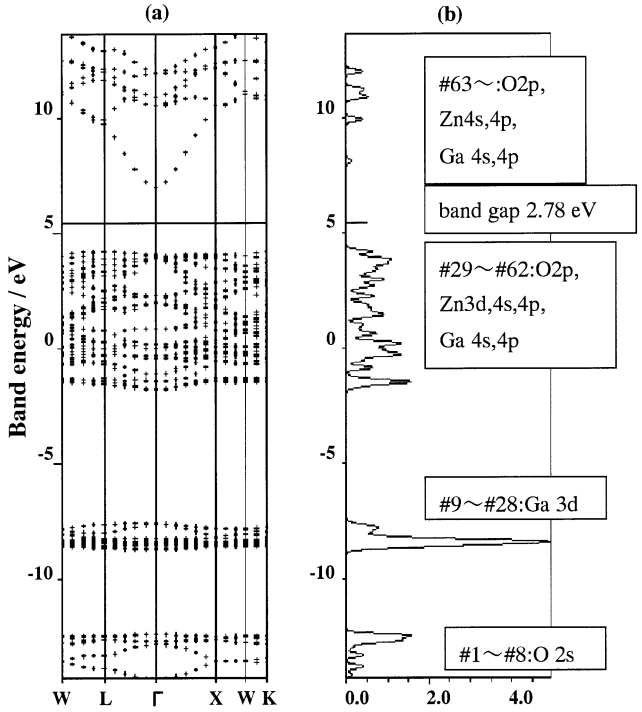

Figure 8. Energy-band diagram (a) and density of states (b) for $ZnGa_2O_4$ calculated by a DFT method.

was composed of O 2p, Ga 4s and 4p, Zn 3d, 4s, and 4p orbitals, whereas the upper part of the band was composed of the O 2p orbitals only. The bottom of the conduction band was composed of the Ga 4s and 4p and Zn 4s and 4p orbitals, as well as a small density of O 2p orbitals again. These individual atomic orbital contributions are discussed in detail in the next session. The band gap was calculated to be 2.78 eV. The energy-band diagram showed large dispersion in the conduction band.

Discussion

The combination of $ZnGa_2O_4$ with RuO_2 produced hydrogen and oxygen under UV irradiation, and the production was quite reproducible in repeated run. About 50-fold turn over number was obtained for 20 h irradiation. These results indicate that water decomposition proceeded photocatalytically on RuO_2-dispersed $ZnGa_2O_4$

The photocatalytic activity increased dramatically in the calcination temperature of $ZnGa_2O_4$ between 1273 and 1373 K. In the same temperature range, the size of $ZnGa_2O_4$ particles observed in the SEM images increased moderately, while the X-ray diffraction peak became sharp with remarkable enhancement of peak intensity and narrow width. Thus, an increase in the activity in the temperature range is associated with the crystallization of $ZnGa_2O_4$, since the promotion of crystallization eliminates impurities and structural imperfections that frequently work as a trap site for photoexcited charges. For calcinations above 1473 K, a sharp decrease in the photocatalytic activity occurred. The SEM images showed the extraordinary growth of $ZnGa_2O_4$ particles. Thus it is likely that the activity decrease is attributed to the reduction of surface area of $ZnGa_2O_4$. In the correlation between RuO_2 amount and photocatalytic activity (Figure 5), a high concentration of RuO_2 amount resulted in a considerable decrease in the activity. This indicates that the excess amount of RuO_2 leads to lower photocatalytic activity. Furthermore, as shown in Figure 2, in the case that the amount of RuO_2 loaded was reduced from 1 to 0.6 wt % for $ZnGa_2O_4$ calcined at as high as 1473 K, the activity increased 5-fold.

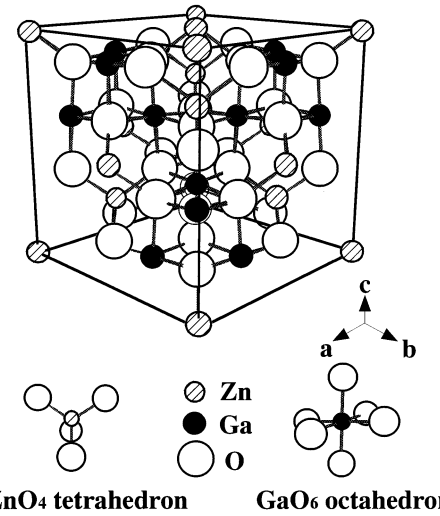

Figure 9. Schematic representation of the crystal structure of $ZnGa_2O_4$.

This result is in agreement with the above-mentioned view that the presence of an excess amount of RuO_2 leads to low activity. Therefore, a decrease in the surface area of $ZnGa_2O_4$ corresponds to a situation similar to the excess amount of RuO_2, as demonstrated in activity decrease in a high concentration of RuO_2.

The X-ray photoelectron spectroscopy showed that the binding energy of Ru $3d_{5/2}$ level for the Ru complex-dispersed $ZnGa_2O_4$ decreased from 281.1 to 280.7 eV when oxidized at 573 K. In a previous XPS study,[2] $RuCl_3$-impregnated $Na_2Ti_6O_{13}$ was oxidized at various temperatures, and measurements of the Ru $3d_{5/2}$ level showed that oxidation at 573−773 K produced Ru species with the binding energy of 280.6−280.7 eV. These values were the same, within experimental accuracy, as that for RuO_2 powder and Ru powder oxidized at 823 K. A comparison with these results indicates that the present Ru species with 280.7 eV is assigned to Ru^{4+}. Since the highest photocatalytic activity was achieved by oxidation at 573 K, irrespective of employment of the different ruthenium compounds as starting materials, it is evident that the Ru species active as a promoter has an oxide form of RuO_2.

As shown in Figure 5, a drastic decrease in photocatalytic activity occurred by oxidation of Ru species at 773 K. The binding energy of the Ru species oxidized at 773 K increased to 280.9 eV. There is a possibility that the positive shift is responsible for changes in the states of RuO_2, although the shift is too small to conclude it. Another possibility is that high-temperature oxidation caused coagulation of RuO_2, producing the assembly of large RuO_2 particles. This leads to lower efficiency for photocatalysis.

Figure 9 shows the schematic representation of $ZnGa_2O_4$ structure. This oxide has a cubic structure with a unit cell of $a = b = c = 833$ pm, and an angle of $\alpha = \beta = \gamma = 90°$.[23] In the structure, Ga^{3+} ions have octahedral coordination, and Zn^{2+} ions are also coordinated tetrahedrally. Thus, a question arises about whether the GaO_6 octahedra exist as a major photocatalytic active site. There is a possibility that the photocatalytic activity might result from the ZnO_4 tetrahedra. To clarify this, the photocatalytic activity for water decomposition of alkaline metal earth gallate, $SrGa_2O_4$, was examined. For 1 wt % RuO_2-loaded $SrGa_2O_4$, hydrogen and oxygen were produced under UV illumination, and its photocatalytic activity was compatible with that of RuO_2-loaded $ZnGa_2O_4$, indicating that the GaO_6 unit in MGa_2O_4 (M = Zn, Sr) is dominantly responsible for photocatalytic activity for water decomposition.

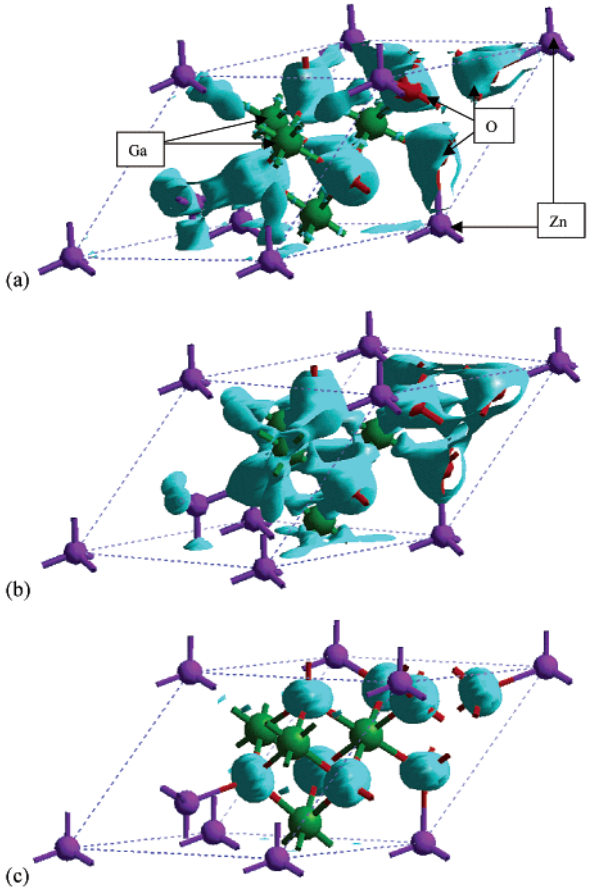

Figure 10. Density contour maps for typical orbitals in the valence band. The primitive unit cell is employed for electronic structure calculations. Zn, Ga, and O atoms are represented by purple, green, and red balls, respectively. (a) Density map collected for orbitals from #29 to #31. Electron density is located in the bonding region between the Zn 3d and O 2p orbitals. (b) Density map for orbital #32. Electron density is located in the bonding region between the Ga 4s4p and O 2p orbitals. (c) Density map for orbital #62, the HOMO. Electron density is simply localized on the O 2p orbitals.

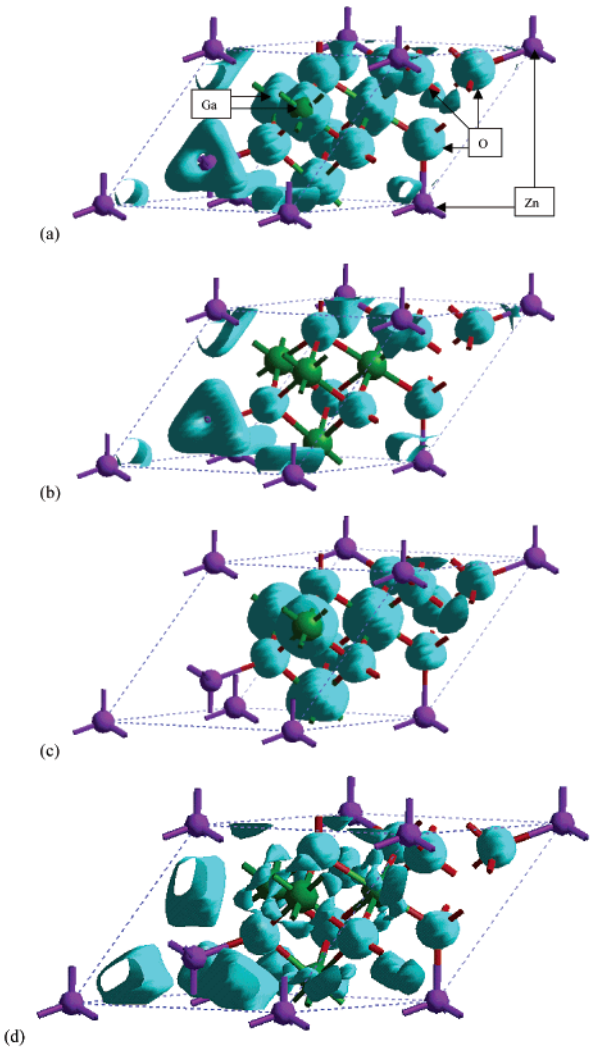

Figure 11. Density contour maps for lower lying orbitals in the conduction band. (a) Density map for orbital #63, i.e., the LUMO. Both Zn 4p(+4s) and Ga 4s(+4p) AO's as well as antibonding mixing of the O 2p AO's are included. (b) Density map for orbital #64. Major electron density is localized on Zn atoms. (c) Density map for orbital #65. Major electron density is localized on Ga atoms. (d) Density map for orbital #69. Electron density is localized on Zn 4p AO's and Ga 4p AO's.

The DFT calculation showed that the valence band consists of 34 orbitals, which correspond to the total number of the Zn 3d and O 2p AO's ($5 \times 2 + 3 \times 8$) (#29 through #62 in our numbering as shown in Figure 8). Figure 10 shows the density contour maps of orbitals for the lower and upper energy parts of the valence band. The lowest energy orbitals at the bottom of valence band (#29 to #31) are composed of the O 2p and Zn 3d AO's, and contribute to the Zn−O bonding as shown in Figure 10a. In the next orbital, #32, the electron density distributes around the Ga and O atoms (Figure 10b). The higher orbitals from #33 through #45 (not illustrated) contribute to the Zn−O bonding, again. Thus, the calculation indicated that the covalent bond character existed between Zn and O atoms, and also between Ga and O atoms to a less degree. From orbitals #46 through #62, the O 2p AO's become nonbonding, and their weight becomes dominant with increasing energy. The orbital #62 is the top of the valence band (HOMO) and is formed by the O 2p AO's only, as shown in Figure 10c. This feature is common to partially covalent semiconductors.

Figure 11 shows the density contour maps of typical orbitals with lower energies in the conduction band. The orbital #63 is the bottom of conduction band (LUMO), and characterized by its large dispersion in the k-space. Figure 11a indicates that this orbital is composed of both the Zn 4s4p and Ga 4s4p AO's as well as O 2p AO's. The triangle-shaped electron density on Zn atom is a clear evidence for inclusion of Zn 4p AO's. The next orbital (#64) and the next-next orbital (#65) are shown in Figure 11b,c, respectively. These orbitals have major electron density on Zn and Ga atoms, respectively. The O 2p AO's always mix into the Zn 4s4p or Ga 4s4p AO's with *out of phase*, which is the counterpart of the *in phase* mixing at the lower energy region of the valance band. Figure 11d shows a still higher orbital #69, which involves dominant contribution from the Zn 4p AO's.

The results indicate that the electron transfer upon illumination occurs from the O 2p AO's to the hybridized orbital of Ga 4s4p and Zn 4s4p AO's. The large overlap among these AO's results in large dispersion of the LUMO, and hence the excited electrons in the conduction band have large mobility, which is considered to be responsible for high photocatalytic performance.

The UV spectra for $ZnGa_2O_4$ showed that main light absorption occurred at 300 nm and attained at the maximum at 250 nm. This absorption wavelength was longer by 20 nm, compared to that of $SrGa_2O_4$. The band gap for $ZnGa_2O_4$ was 4.3 eV which was smaller than 4.7 eV for $SrGa_2O_4$. Sampath

et al. used the tight-binding muffin-tin orbital method for the calculation of the electronic structures of $ZnGa_2O_4$.[24] The band-gap was estimated to be 2.79 eV, which was in a good agreement with 2.78 eV obtained in the present study. For the II−VI semiconductors, Wei and Zunger pointed out that the p−d repulsion repels the valence band maximum upward without affecting the conduction minimum.[25] Sampath et al. also showed that the hybridization of Zn 3d with the O 2p orbitals shifts the valence-band maximum upward.[24] Furthermore, since $ZnGa_2O_4$ has two 3d bands of Zn and Ga elements, the presence of Ga 3d band in addition to the Zn 3d band in the upper valence band further provides the p−d repulsion for the valence-band maximum, reducing the band gap. Thus, one possibility for narrower band gap for $ZnGa_2O_4$ than for $SrGa_2O_4$ is the p−d repulsion. The other possibility is asked for the conduction band. The bottom of the conduction band is composed of the Zn−Ga hybridized orbitals for $ZnGa_2O_4$ but of Ga 4s4p AO's only for $SrGa_2O_4$. It is likely that the strong mixing of Zn and Ga orbitals in the conduction band of $ZnGa_2O_4$ are also responsible for the narrow band gap, as indicated by large dispersion in the DOS.

In the transition metal oxides of Ti^{4+}, Nb^{5+}, and Ta^{5+} ions, their valence bands are composed of the O 2p orbital. Thus, the character of valence band in $ZnGa_2O_4$ is the same as that in the transition metal oxides. However, it should be noted that the distinctive electronic structure of $ZnGa_2O_4$ different from the transition metal oxides can be seen in the conduction band. In the transition metal oxides, the vacant narrow d orbitals are responsible for the conduction bands, whereas the broad hybridized Zn 4s4p and Ga 4s4p orbitals are important in $ZnGa_2O_4$. Thus, the characteristic feature of $ZnGa_2O_4$ is that the diffuse 4s and 4p orbitals contribute as an electron acceptor to photocatalysis.

Solid photocatalysts so far discovered for water decomposition have been composed of the octahedrally coordinated d^0 transition metal ions involving Ti^{4+}, Zr^{4+}, Nb^{5+}, and Ta^{5+}. The present study showed that RuO_2-dispersed $ZnGa_2O_4$ involving Ga^{3+} with d^{10} configuration has the ability to photocatalytically decompose water to H_2 and O_2. In previous studies, we have demonstrated that three kinds of the p-block metal ions (In^{3+}, Sn^{4+}, and Sb^{5+}) with d^{10} configuration make a good photocatalyst for water decomposition when combined with RuO_2.[3−5,15−17] By adding the present results to the previous ones, the p-block metal oxide group having a metal ion with d^{10} configuration is concluded to form a series of the photocatalysts, in addition to the conventional metal oxides with a transition metal ion of d^0 configuration.

Acknowledgment. This work was supported by CREST of JSP.

References and Notes

(1) Domen, K.; Kudo, A.; Onishi, T. *J. Catal.* **1986**, *102*, 92.
(2) Inoue, Y.; Kubokawa, T.; Sato, K. *J. Phys. Chem.* **1991**, *95*, 4059.
(3) Ogura, S.; Kohno, M.; Sato, K.; Inoue, Y. *Appl. Surf. Sci.* **1997**, *121/123*, 521.
(4) Inoue, Y.; Asai, Y.; Sato, K. *J. Chem. Soc., Faraday Trans.* **1994**, *90*, 797.
(5) Kohno, M.; Kaneko, T.; Ogura, S.; Sato, K.; Inoue, Y. *J. Chem. Soc., Faraday Trans.* **1998**, *94*, 89.
(6) Takata, T.; Furumi, Y.; Shinohara, K.; Tanaka, A.; Hara, M.; Kondo, J. N.; Domen, K. *Chem. Mater.* **1997**, *9*, 1063.
(7) Takata, T.; Shinohara, K.; Tanaka, A.; Hara, M.; Kondo, J. N.; Domen, K. *J. Photochem. Photobiol. A: Chem.* **1997**, *106*, 45.
(8) Sayama, K.; Arakawa, H. *J. Phys. Chem.* **1993**, *97*, 531.
(9) Kudo, A.; Tanaka. A.; Domen, K.; Maruya, K.; Aika, K.; Onishi, T. *J. Catal.* **1998**, *111*, 67.
(10) Kudo, A.; Kato, H; NakaGawa, S. *J. Phys. Chem. B* **2000**, *104*, 571.
(11) Kato, H.; Kudo, A. *Catal. Lett.* **1999**, *58*, 153.
(12) Ishihara, T.; Nishiguchi, H.; Fukamachi, K.; Takita, Y. *J. Phys. Chem. B* **1999**, *103*, 1.
(13) Kato, H.; Kudo, A. *Chem. Phys. Lett.* **1998**, *295*, 487.
(14) Kato, H.; Kudo, A. *Chem. Lett.* **1999**, 1027.
(15) Ogura, S.; Kohno, M.; Sato, K.; Inoue, Y. *Phys. Chem. Chem. Phys.* **1999**, *1*, 179.
(16) Kohno, M.; Ogura, S.; Sato, K.; Inoue, Y. *J. Chem. Soc., Faraday Trans.* **1997**, *93*, 2433.
(17) Kohno, M.; Ogura, S.; Sato, K.; Inoue, Y. *Chem. Phys. Lett.* **1997**, *267*, 72.
(18) Sato, J.; Saito, S.; Nishiyama, H.; Inoue, Y. *J. Phys. Chem.* **2001**, *105*, 6061.
(19) Sato, J.; Saito, S.; Nishiyama, H.; Inoue, Y. *Chem. Lett.* **2001**, 868.
(20) Sato, J.; Saito, S.; Nishiyama, H.; Inoue, Y. *J. Photochem. Photobiol. A: Chem.* **2002**, *148*, 85.
(21) JCPDS file, 38-1240.
(22) Payne, M. C.; Teter, M. P.; Allan, D. C.; Arias, T. A.; Joannopoulos, J. D. *Rev. Mod. Phys.* **1992**, *64*, 1045.
(23) Hornstra, J.; Keulen, E. *Phillips Res. Rep.* **1972**, *27*, 76.
(24) Sampath, S. K.; Kanhere, D. G.; Pandey, R. J. *Phys.: Condens. Matter* **1999**, *11*, 3635.
(25) Wei. S. H.; Zunger, A. *Phys. Rev.* **1988**, *B37*, 8958.